Composite Structures 131 (2015) 742–752

Contents lists available at ScienceDirect

Composite Structures

journal homepage: www.elsevier.com/locate/compstruct

Design optimization and manufacture of hybrid glass/carbon fiber reinforced composite bumper beam for automobile vehicle

Do-Hyoung Kim [a], Hyun-Gyung Kim [b], Hak-Sung Kim [a,c,*]

[a] Department of Mechanical Convergence Engineering, Hanyang University, Haengdang-dong, Seongdong-gu, Seoul 133-791, South Korea
[b] Department of Advanced Trim Engineering, Hyundai Motors, Hwaseong-si, Gyeonggi-do 445-706, South Korea
[c] Institute of Nano Science and Technology, Hanyang University, Seoul 133-791, South Korea

ARTICLE INFO

Article history:
Available online 19 June 2015

Keywords:
Fiber reinforced composite
Hybrid glass/carbon fiber composite
Impact simulation
Finite element analysis
Optimal design

ABSTRACT

In this study, the hybrid glass/carbon composite bumper beam was designed and manufactured via the design optimization process combined with the impact analysis. The glass/carbon mat thermoplastic (GCMT) composite was devised to substitute for the conventional glass mat thermoplastic (GMT) for reducing the weight of bumper beam. For the design optimization, the mechanical properties of GCMT were predicted and the optimal design of bumper beam was performed with the impact simulation. Based on the final design, the real bumper beam was manufactured and its impact performances were measured. It was found that the optimally designed GCMT bumper beam had 33% less weight compared to the conventional GMT bumper beam while having the improved impact performances.

1. Introduction

Nowadays, fuel efficiency in automotive industry has become the main issue since the engine emissions have recognized as a major source of air pollution [1]. To improve fuel efficiency, many attempts have been tried by many researchers to replace the heavy metallic material of the automotive components with lighter materials such as aluminum or magnesium alloy, ultra-high strength steel or fiber reinforced plastic (FRP) composites [2,3]. Especially, the glass fiber reinforced plastic (GFRP) and the carbon fiber reinforced plastic (CFRP) composites have received much attention for automotive structures due to their high specific stiffness, high specific strength and high damping capability compared to the conventional metallic materials [1,2]. Using these advantages, the weight of automotive structural parts could be reduced without any degradation of mechanical performances [4]. Also, many attempts of FRP applications in the automotive component have been tried not only for the exterior parts of an automobile but also for the interior parts which sustain heavy loads during various driving conditions [5].

A bumper beam is one of the parts of bumper system which protects the passengers from the crash by absorbing the impact energy. Fig. 1 shows the schematic of automotive bumper system. In recent years, the glass mat thermoplastic (GMT) which consisted of unidirectional GFRP layers and the woven form of GFRP layers has been commonly employed for the material of bumper beam because it has excellent absorbing capacity of impact energy while has lower weight than that of the conventional metallic materials [6]. Moreover, CFRP is also being considered as the new material of bumper beam to reduce weight of bumper beam because CFRP has the higher specific strength under high impact load compared to the GFRP [7]. However, the carbon fiber is too much expensive to replace entire structure of bumper beam compared to the glass fiber composites. Considering the material cost, it may be the best design that the composing of carbon fiber and the glass fiber together into the bumper beam to reduce the weight and improve the impact performance, simultaneously.

In this study, design of the hybrid glass/carbon composite bumper beam was carried out. The hybrid glass/carbon mat thermoplastic (GCMT) which is composed of unidirectional and woven form of glass/carbon fiber reinforced plastic layers, was used to replace the conventional GMT composite. The mechanical properties of GCMT were predicted using the classical laminate plate theory (CLPT) and finite element analysis (FEA). Then the optimal design of bumper beam was performed with the impact simulation. Based on the final design result, the real bumper beam was manufactured and its impact performances were measured.

* Corresponding author at: Department of Mechanical Convergence Engineering, Hanyang University, Haengdang-dong, Seongdong-gu, Seoul 133-791, South Korea. Tel.: +82 2 2220 2898.
E-mail address: kima@hanyang.ac.kr (H.-S. Kim).

http://dx.doi.org/10.1016/j.compstruct.2015.06.028
0263-8223/

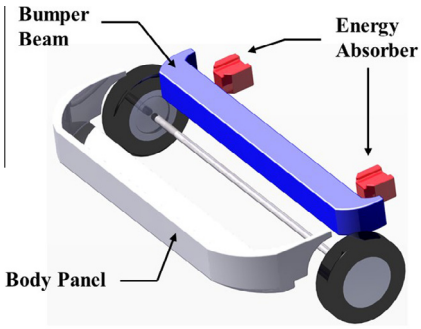

Fig. 1. The schematic of bumper system.

2. Calculation of the mechanical properties of glass/carbon mat thermoplastic (GCMT)

2.1. Conventional GMT and newly designed GCMT

Fig. 2 shows the structure of conventional GMT consisted of unidirectional (UD) glass fiber layers and woven glass fiber layer, which has been typically used by Hyundai Motors for the material of bumper beam. For the matrix and fiber of GMT, the polypropylene (PP) and the E-glass were used, respectively. Also, the commercial woven glass weave Twintex (Twintex® PP60, Fiber Glass Industries, USA) was used for composing of the woven layer. The volume fraction of glass fiber of each layer was given in Table 1. In this work, some of the glass fibers were replaced with the carbon fibers to reduce the weight of bumper beam while improving the impact performances. The new designs of the GCMT were chosen as following lists (Fig. 3). Case 1, 50% of glass fibers in UD layer were substituted by carbon fiber. Case 2, all of glass fibers in UD layer were replaced by carbon fibers. Case 3, 50% of longitudinal glass fiber yarns in woven layer were replaced by carbon fiber. Case 4, all of longitudinal glass fiber yarns in woven layer were replaced by carbon fiber. For all of the cases, the carbon fiber T-300 was used for substitution. The mechanical properties of fibers and matrix are listed in Table 2.

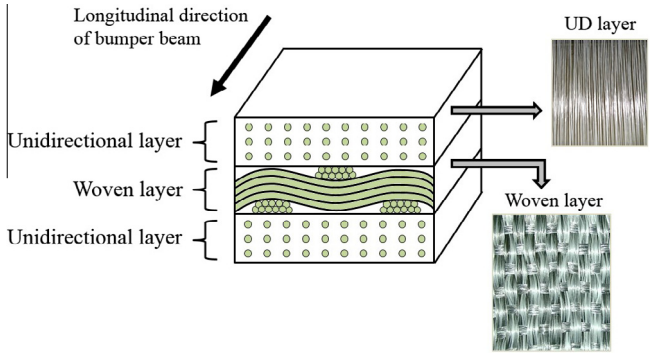

Fig. 2. Structure of conventional GMT (glass mat thermoplastic).

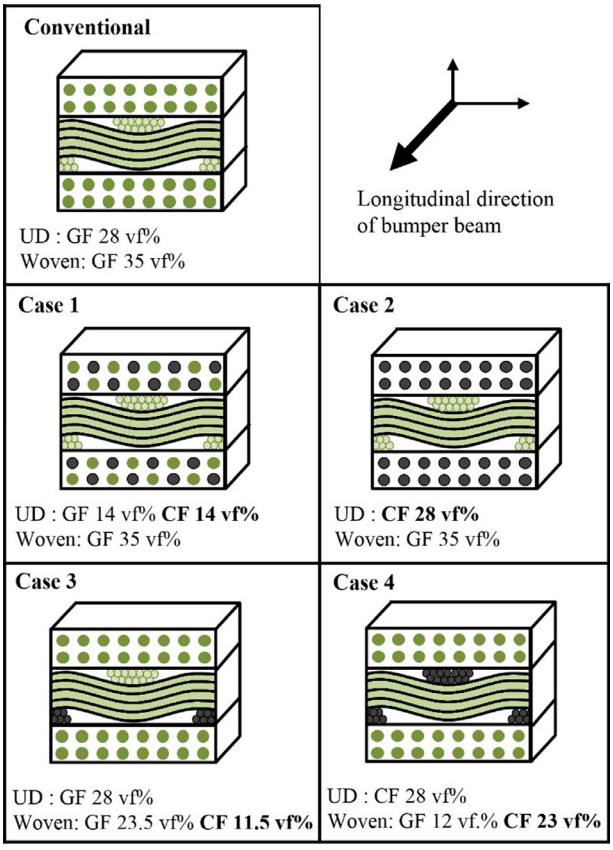

Fig. 3. New designs of GCMT (glass/carbon mat thermoplastic).

2.2. Mechanical properties of UD layer

In this work, the mechanical properties of UD layer were calculated for each design case. Firstly, the density and moduli were obtained by using the rule of mixtures (ROM). The experimental evidences have been reported that the ROM provides accurate prediction of the effective modulus of UD composite over a wide range of fiber volume fraction [8]. By using ROM, the density and elastic properties were calculated as following equations:

$$\begin{aligned} \rho &= \rho_F V_F + \rho_M V_M \\ \nu_{12} &= \nu_F V_F + \nu_M V_M \\ E_{11} &= E_{11F} V_F + E_M V_M \\ \frac{1}{E_{22}} &= \frac{V_F}{E_{22F}} + \frac{V_M}{E_M} \\ \frac{1}{G_{12}} &= \frac{V_F}{G_{12F}} + \frac{V_M}{G_M} \end{aligned} \quad (1)$$

where ρ is the density, V is the volume fraction of fiber, E_{11} and E_{22} are elastic moduli of longitudinal direction and transverse direction, ν is poisson's ratio, G_{12} are shear modulus. The subscripts F and M represent the fiber and matrix, respectively.

Then, the strength properties of UD layer were calculated as following. For the shear and longitudinal tensile strength, the modified ROM was used for prediction which is employing the

Table 1
Information of unidirectional and woven GF layer in conventional GMT.

	Type of glass fiber	Type of matrix	Glass fiber volume fraction (%)	Tex	Fabric type
Woven layer	E-glass	Polypropylene	35	1870	4/1 Plain weave
Unidirectional layer	E-glass	Polypropylene	14 (for each layer)	–	–

Table 2
Mechanical properties of materials used in GCMT.

Materials	Density (10^3 kg/m^3)	Longitudinal modulus E_{11} (GPa)	Transverse modulus E_{22} (GPa)	Shear Modulus G_{12} (GPa)	Poisson's ratio ν_{12}	Longitudinal tensile strength X^t (MPa)	Longitudinal compressive strength X^c (MPa)
E-glass fiber	2.49	75	75	30	0.2	1860	–
Carbon fiber (T-300)	1.77	220	14	9	0.2	3650	–
PP	0.905	1.34	1.34	0.757	0.45	33	48

effective fiber volume fraction to consider the non-linear strength degradation [9]. The effective fiber volume fraction V_{EF} is calculated as follows:

$$V_{EF} = V_F(1 - P) \tag{2}$$

where V_F is the fiber volume fraction and P is the degradation parameter determined as following:

$$\begin{aligned} P &= 0.4333 - 0.4888V_F \quad \text{for } V_F < 0.54 \\ P &= -0.2629 + 0.8006V_F \quad \text{for } V_F \geqslant 0.54 \end{aligned} \tag{3}$$

Then, the longitudinal tensile strength X^T and shear strength S_{12} are calculated as follows:

$$\begin{aligned} X^T &= \sigma'_M V_M + \sigma_F V_{EF} \\ S_{12} &= \tau'_M V_M + \tau_F V_{EF} \end{aligned} \tag{4}$$

where σ'_M and τ'_M are the matrix strength at the failure strain of fiber, σ_F and τ_F are the ultimate tensile and shear strength of fiber, respectively.

The longitudinal compressive strength X^C was calculated using the Budiansky model [10] which is assumed that the compressive failure is a result of yielding of plastic shear deformation due to misaligned fibers within a certain band. The expression of Budiansky model following as:

$$X^C = \frac{G_s}{1 + \bar{\phi}/\gamma_y}, \quad G_s = \frac{G_M}{V_M} \tag{5}$$

where $\bar{\phi}$ is the initial fiber misalignment, γ_y is the shear yield strain of composites and G_s is the effective shear modulus, respectively. In this work, the constant value 4 was used for $\bar{\phi}/\gamma_y$ because the value of $\bar{\phi}/\gamma_y$ is close to 4 under the elastic behavior, based on the result of Budiansky and Fleck [10].

It had been reported that the transverse strengths almost depend on the mechanical properties of matrix [11,12]. The transverse tensile strength Y^T and compressive strength Y^C can be predicted as following equations [13]:

$$\begin{aligned} Y^T &= \left[1 - \left(\sqrt{V_F} - V_F\right)(1 - E_M/E_{22F})\right]\sigma_M^T \\ Y^C &= \left[1 - \left(\sqrt{V_F} - V_F\right)(1 - E_M/E_{22F})\right]\sigma_M^C \end{aligned} \tag{6}$$

where σ_M^T and σ_M^C are the ultimate tensile strength and compressive strength of matrix, respectively.

2.3. Prediction of mechanical properties of woven layer

The mechanical properties of woven fabric layer were obtained by virtual tests using FEA method. First, the unit cell of woven fabric was modeled by using commercial CAD software (CATIA V5, Dassault Systems, USA). Fig. 4a depicts the 4/1 plane weave woven fabric used in GMT and its unit cell which is the smallest repeated area periodically. Using the symmetric surface of unit cell, the half part of unit cell was modeled for the simulation as shown in Fig. 4b and c. The outer dimension and thickness were determined by measuring of manufactured woven fabric. The dimensions of warp and fill of fibers were adjusted for the fibers having 35% of volume fraction which is same to the conventional woven layer. The fibers were modeled simply with linear line of cross-section of warp and fill, without geometrical complexity in order to save computing time of simulation. Then the matrix part could be modeled by excluding the fiber part from entire rectangular part. After the assembling of fiber and matrix part, the finite element meshes (1296 elements of C3D8R and 2093 of C3D4) were generated automatically using commercial FEA software ABAQUS 6.10 (Hibbit, Karlsson & Sorensen, USA) as shown in Fig. 5. The interfaces between the fibers and the matrix were assumed as perfect bonding for the simple calculation. In the virtual tests of unit cell, longitudinal, transverse and shear mechanical properties were obtained with respect to the directions of force applied as shown in Fig. 5. To obtain the strength properties, it was assumed that the unit cell would be failed when the stress in the fiber or matrix reaches to their failure strength during the force was applied. For all of cases, the displacement in the thickness direction (z-axis) was fixed.

2.4. Mechanical properties of entire structure of GCMT

The mechanical properties of entire structure of GCMT were calculated by using the classical laminated plate theory (CLPT) based on the obtained mechanical properties of each layer. It has been known that the CLPT is a common approach method used to predict mechanical properties, especially for the thin plate composite structures [14]. In the CLPT, individual laminate are assumed to be homogeneous and orthotropic. When there are no hydrothermal effects, the analytical stiffness of composite laminate is expressed as following:

$$\begin{Bmatrix} N_x \\ N_y \\ N_{xy} \\ M_x \\ M_y \\ M_{xy} \end{Bmatrix} = \begin{bmatrix} A_{11} & A_{12} & A_{16} & B_{11} & B_{12} & B_{16} \\ A_{12} & A_{22} & A_{26} & B_{12} & B_{22} & B_{26} \\ A_{16} & A_{26} & A_{66} & B_{16} & B_{26} & B_{66} \\ B_{11} & B_{12} & B_{16} & D_{11} & D_{12} & D_{16} \\ B_{12} & B_{22} & B_{26} & D_{12} & D_{22} & D_{26} \\ B_{16} & B_{26} & B_{66} & D_{16} & D_{26} & D_{66} \end{bmatrix} \begin{Bmatrix} \varepsilon_x^0 \\ \varepsilon_y^0 \\ \gamma_{xy}^0 \\ \kappa_x \\ \kappa_y \\ \kappa_{xy} \end{Bmatrix} \tag{7}$$

where N_x, N_y, N_{xy} are in-plane forces per unit length, M_x, M_y, M_{xy} are moments per unit length, ε_x^0, ε_y^0, γ_{xy}^0 are the strains of midplane and κ_x, κ_y, κ_{xy} are the plate curvatures. $[A]$ is the in-plane stiffness matrix, $[B]$ is stretching-bending coupling matrix and $[D]$ is the bending stiffness matrix. When the stacking sequence of a laminate is symmetric about its midplane, the bending–stretching coupling matrix $[B]$ is identically zero. Also, this laminate is subjected to in-plane force $\{N\}$ only, the curvature $\{\kappa\}$ reduces to zero. Then, Eq. (7) become

$$\begin{Bmatrix} N_x \\ N_y \\ N_{xy} \end{Bmatrix} = \begin{bmatrix} A_{11} & A_{12} & A_{16} \\ A_{12} & A_{22} & A_{26} \\ A_{16} & A_{26} & A_{66} \end{bmatrix} \begin{Bmatrix} \varepsilon_x^0 \\ \varepsilon_y^0 \\ \gamma_{xy}^0 \end{Bmatrix} \tag{8}$$

and the in-plane stiffness matrix $[A]$ can be calculated as following:

$$A_{ij} = \sum_{k=1}^{N} [\overline{Q}_{ij}]^{[k]} (z_k - z_{k-1}) \tag{9}$$

where $[\overline{Q}_{ij}]^{[k]}$ are the transformed reduced stiffness of the kth ply and the z_k represents the displacement between midplane and kth

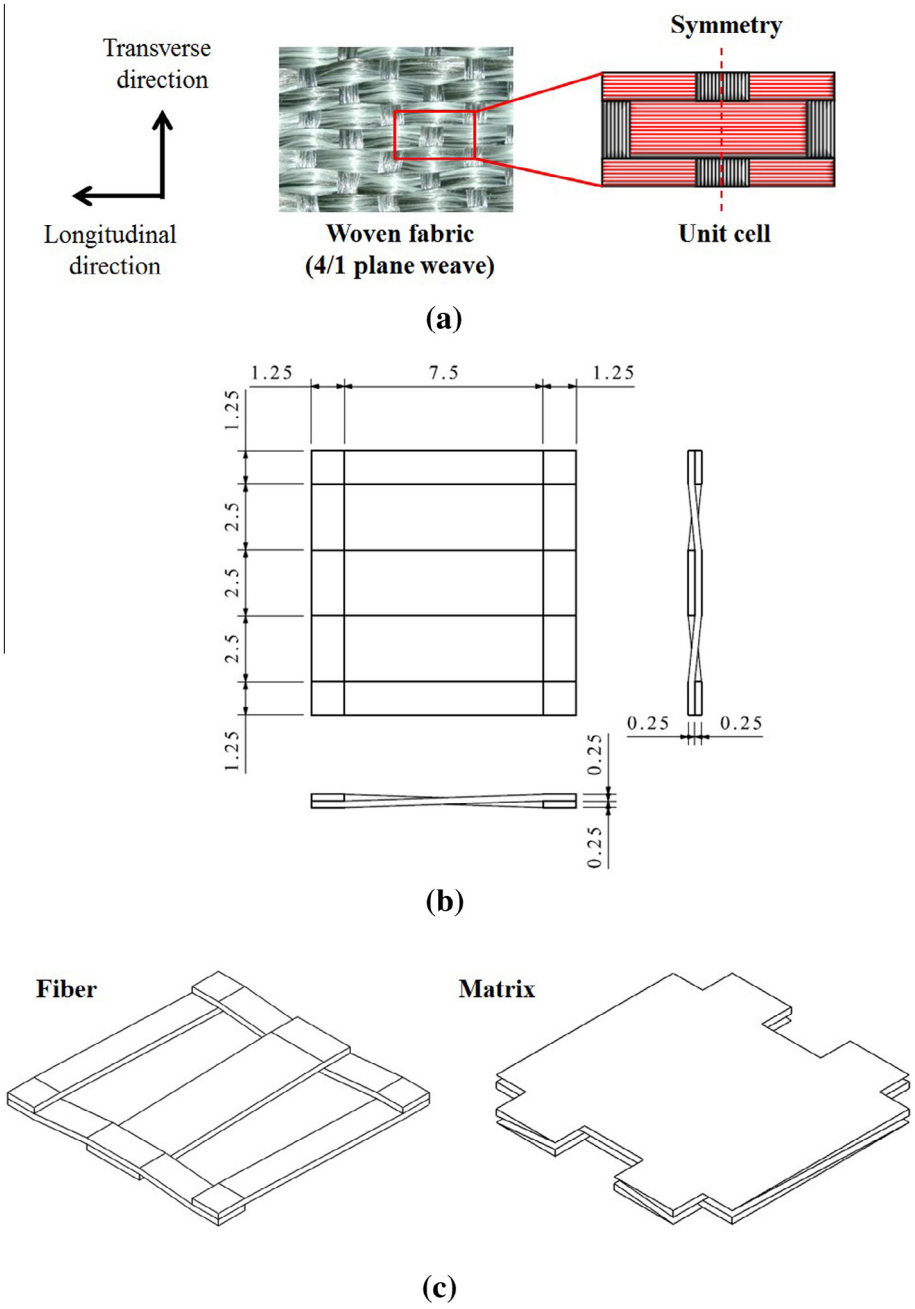

Fig. 4. Modeling of woven layer: (a) unit cell of woven fabric; (b) geometry of fiber model; (c) 3D view of fiber and matrix model composing unit cell.

ply. Then, the elastic properties of entire GCMT laminate are calculated as follows:

$$E_x = \frac{|A|}{h\left(A_{22}A_{66} - A_{26}^2\right)}, \quad E_y = \frac{|A|}{h\left(A_{11}A_{66} - A_{16}^2\right)}, \quad G_{xy} = \frac{|A|}{h\left(A_{11}A_{22} - A_{12}^2\right)}$$
$$v_{xy} = -\frac{A_{16}A_{26} - A_{12}A_{66}}{A_{22}A_{66} - A_{26}^2}, \quad v_{yx} = -\frac{A_{16}A_{26} - A_{12}A_{66}}{A_{11}A_{66} - A_{16}^2} \tag{10}$$

where $|A|$ is determinant of $[A]$, E_x, E_y, G_{xy} are axial, transverse, shear modulus of the laminate and v_{xy}, v_{yx} are poisson's ratio.

For the calculation of strength properties of GCMT, the maximum stress failure criterion was used for the simple calculation. In the case of one directional virtual loading tests used to characterize the material properties, it has been known that the maximum stress criterion can be the appropriate prediction method because the off-axis stress is much smaller than the axis stress thus effect of multi-axial stress can be neglected [8,15,16]. The maximum stress criterion predicts the failure of composite when the any component of stress in kth layer ($\sigma_1^{[k]}$, $\sigma_2^{[k]}$, $\tau_{12}^{[k]}$) exceeds the failure strength. It is expressed as follows:

$$\begin{aligned} X^C < \sigma_1^{[k]} < X^T \\ Y^C < \sigma_2^{[k]} < Y^T \\ \left|\tau_{12}^{[k]}\right| < S_{12} \end{aligned} \tag{11}$$

where X^C and X^T are compressive and tensile ultimate strength in fiber direction, Y^C and Y^T are compressive and tensile ultimate strength in transverse direction and S_{12} is the ultimate shear strength.

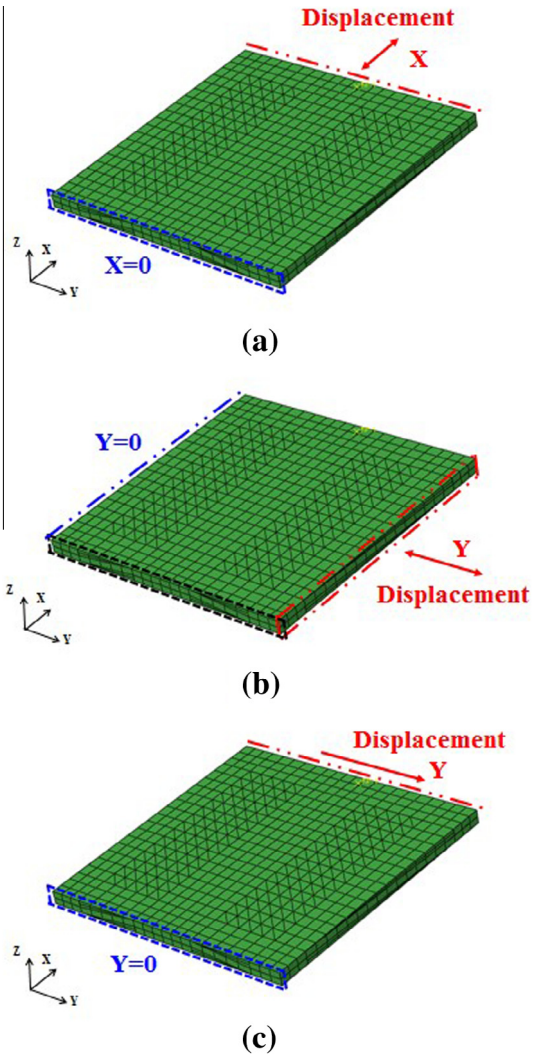

Fig. 5. Finite element model of the unit cell and virtual test conditions: (a) for longitudinal properties; (b) for transverse properties; (c) for shear properties.

2.5. Verification of calculation procedure for conventional GMT

To verify the mechanical property calculation scheme used in this study, experimental tests for the conventional GMT were performed. The GMT specimens for uniaxial, compressive and shear tests were fabricated based on ASTM standard D3039, D3410 and D5379, respectively. The all of tests were carried out by using universal testing machine (UNITECH, R&B, South Korea). The unsupported gage zig was used for the compression test and the V-notched beam method was employed for the shear test, respectively. Fig. 6 shows the geometry of specimen for V-notched beam method. For all of test, five specimens were tested for the reliable experimental results.

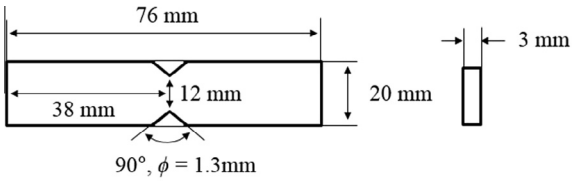

Fig. 6. Geometry of composite specimen for shear test using V-notched beam method.

3. Impact simulation of bumper beam

To evaluate the impact performances of GCMT bumper beam, the impact simulations were performed by using LS-DYNA (LSTC, USA). In this work, the standard of Insurance Institute for Highway safety (IIHS) [17] was used to evaluate the impact performance of bumper beam which is employed in Hyundai Motors. IIHS bumper impact barrier test is representatively used to measure the standard damage requirement as the low-speed crash. As shown in Fig. 7, the IIHS bumper barrier impact test is composed of bumper system and impact barrier where the bumper system with beam is impacted by the impact barrier at 10 km/h.

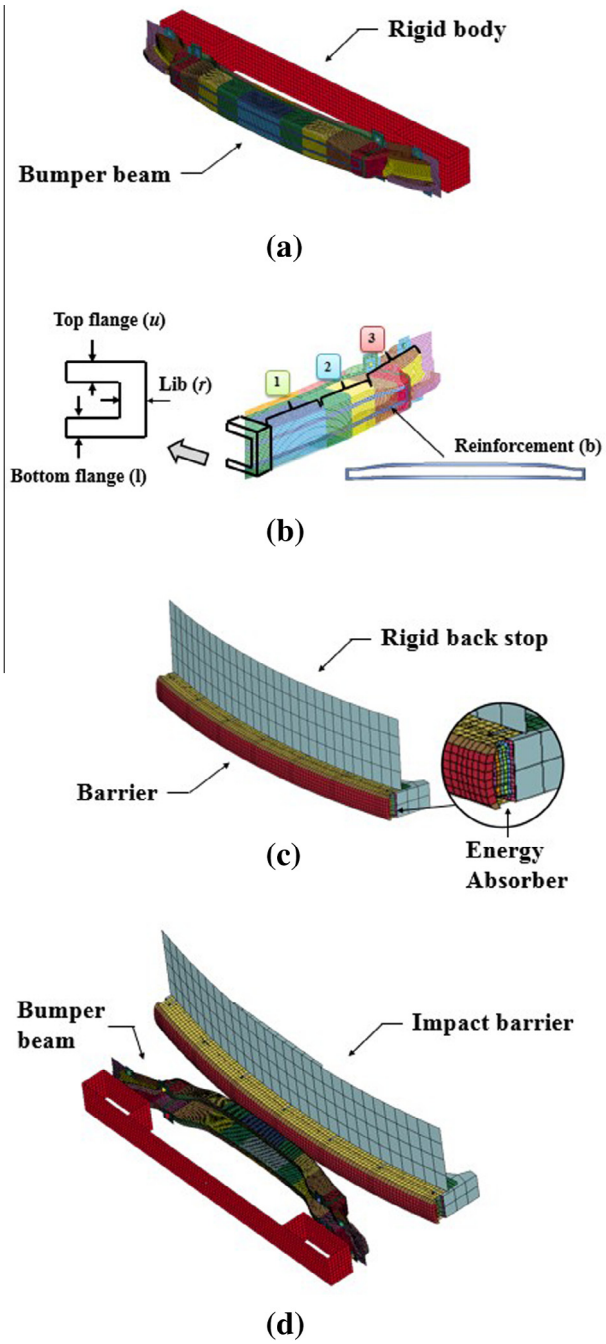

Fig. 7. Simulation for IIHS bumper barrier impact test and its FEA models: (a) bumper system; (b) impact barrier (c) full model of impact simulation; (d) parts of bumper beam.

The specification of impact barrier was referred in IIHS bumper test protocol which is consisted of barrier, energy absorber and rigid back stop. In this work, the impact simulation was considered as desirable analysis technique because it can describe the real impact test exactly although it could be the time consuming technique compared to the other approach such as the response modeling technique [18–20]. The impact simulation has advantages that the analysis results can be directly compared with result of impact test and also the failure load, position and mode were can be predicted and analyzed with the composite failure criterion. For the FEA analysis, the meshes (39391 4-node Belytschko-Tsay shell elements with the five integration points through shell thickness) were generated from the geometrical model supported by Hyundai Motors. As shown in Fig. 7d, the bumper beam is consisted of 10 parts which are the bumper beam reinforcements, 3 parts of each top, lib and bottom flange. Thickness of each part was selected as the design variables for the optimization procedure to minimize the weight of bumper beam. The detail information of optimal design is described in Section 4.

In IIHS bumper test, the impact performance of bumper system is evaluated by measuring the deflection and intrusion as shown in Fig. 8. The deflection is defined as the maximum inside deformation of bumper beam after the crash. Low deflection is needed for bumper system because the deformed bumper beam should not make any contact with other components of automotive after the crash for the safety of passenger [21]. The intrusion is defined as a maximum relative distance between the bumper beam and impact barrier during the crash and low intrusion is desirable to reduce the injury risk of person hit by automotive [22]. During the impact simulation, the intrusion and deflection were obtained from the distance between nodes of bumper beam and impact barrier. In this work, 3 middle node sets on front surface of bumper beam were selected as the measuring points (Fig. 8b) and highest value was defined as the intrusion and deflection result after the impact simulation. Additionally, the failure of bumper beam during impact simulation was predicted by using Tsai-Wu criterion [23]. The Tsai-Wu criterion predicts the failure of composite when the failure index f_i in a laminate reaches one as follows:

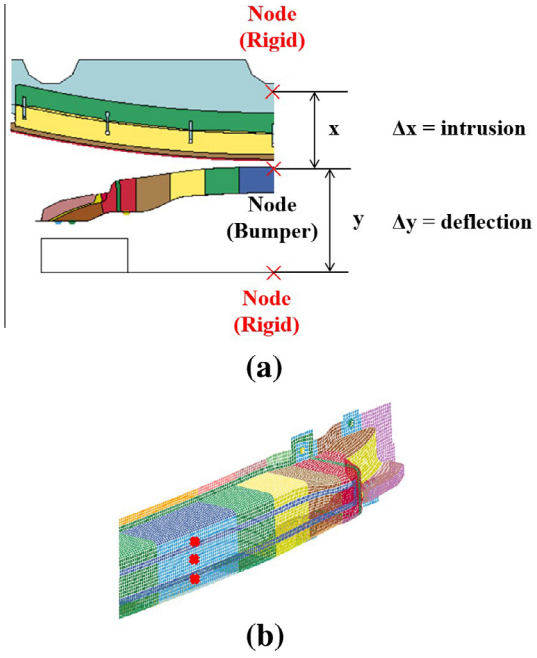

Fig. 8. The definition of intrusion and deflection: (a) intrusion and deflection; (b) selected nodes.

$$f_i = F_i\overline{\sigma}_i + F_{ij}\overline{\sigma}_i\overline{\sigma}_j = 1, \quad i, j = 1, 2, 6 \tag{12}$$

where $\overline{\sigma}_i$ and $\overline{\sigma}_j$ represent the stress components at failure, and the F_{ij} are expressed in terms of the strength values of the material in tension, compression, and shear. For a single lamina in plane stress, (12) reduces to

$$f_i = F_1\overline{\sigma}_1 + F_1\overline{\sigma}_2 + F_{11}\overline{\sigma}_1^2 + F_{22}\overline{\sigma}_2^2 + F_{66}\overline{\sigma}_6^2 + 2F_{12}\overline{\sigma}_1\overline{\sigma}_2 = 1 \tag{13}$$

The Tsai-Wu coefficients are defined as follows:

$$F_1 = \frac{1}{X^T} + \frac{1}{X^C}, \quad F_2 = \frac{1}{Y^T} + \frac{1}{Y^C}, \quad F_{11} = -\frac{1}{X^T X^C}, \quad F_{22} = -\frac{1}{Y^T Y^C}$$
$$F_{66} = \frac{1}{S_{12}^2}, \quad F_{12} = -0.5\sqrt{F_{11}F_{22}} \tag{14}$$

The impact simulation was performed with 10 km/h of initial velocity of bumper beam based on IIHS impact test standard. All surfaces of bumper beam and rigid body were defined as one contact group for effective calculation of multiple contacting during impact analysis. In the case of conventional GMT bumper beam, the 136 mm of intrusion and 93.6 mm of deflection were obtained. These conventional impact performances were reflected to specify the constraint of optimal design in Section 4.

4. Design optimization of the hybrid bumper beam

4.1. Design requirement and variables

The design requirement for hybrid bumper beam was to minimize the weight with maintaining of impact performances. The weight of bumper beam depends on the material and thickness of bumper beam parts. The mass of the bumper beam m_b was calculated as:

$$m_b = \rho_{com} \times \sum_{i=1}^{n} (A_{surface,i} \times t_{part,i}) \tag{15}$$

where ρ_{com} is the density of material, n is the number of bumper beam part, $A_{surface,i}$ is the surface area and $t_{part,i}$ is the thickness of ith part, respectively. The shell surface area was calculated automatically in analysis step in LS-DYNA. To minimize the weight of bumper beam, the following objective function was used:

$$\textit{Minimize} \quad m_b \tag{16}$$

Also, the impact performance of bumper beam should be maintained compared to the conventional GMT bumper beam as following:

$$\begin{aligned} &\text{Intrusion} \le 136 \text{ mm} \\ &\text{Deflection} \le 93.6 \text{ mm} \end{aligned} \tag{17}$$

For the design variables, each thickness of 3 parts of top flange (u_1, u_2, u_3), front rib (r_1, r_2, r_3), bottom flange (l_1, l_2, l_3) and thickness of bumper reinforcement (b) were selected as shown in Fig. 7d. Because the bumper beam consists of 10 parts with complex shapes, it is too difficult to control the each part of bumper beam by decimal point of thickness. Therefore, to consider the manufacturing condition of bumper beam based on the result of optimal design, the discrete values were used for each design variable. In this work, each design variable was allowed to have one of the following discrete values as 3, 4, 5, . . ., 14.

4.2. Design problem formulation

Combining the design requirements described in Section 4.1 and the design variables described in Section 4.2, we could formulate the discrete design optimization problem as following:

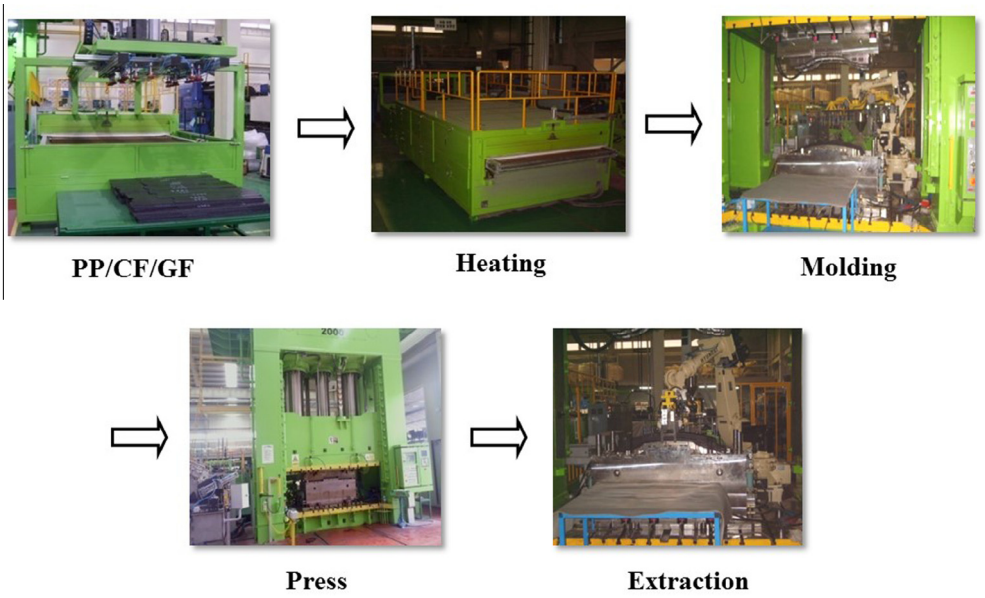

Fig. 9. Manufacturing process of hybrid bumper beam.

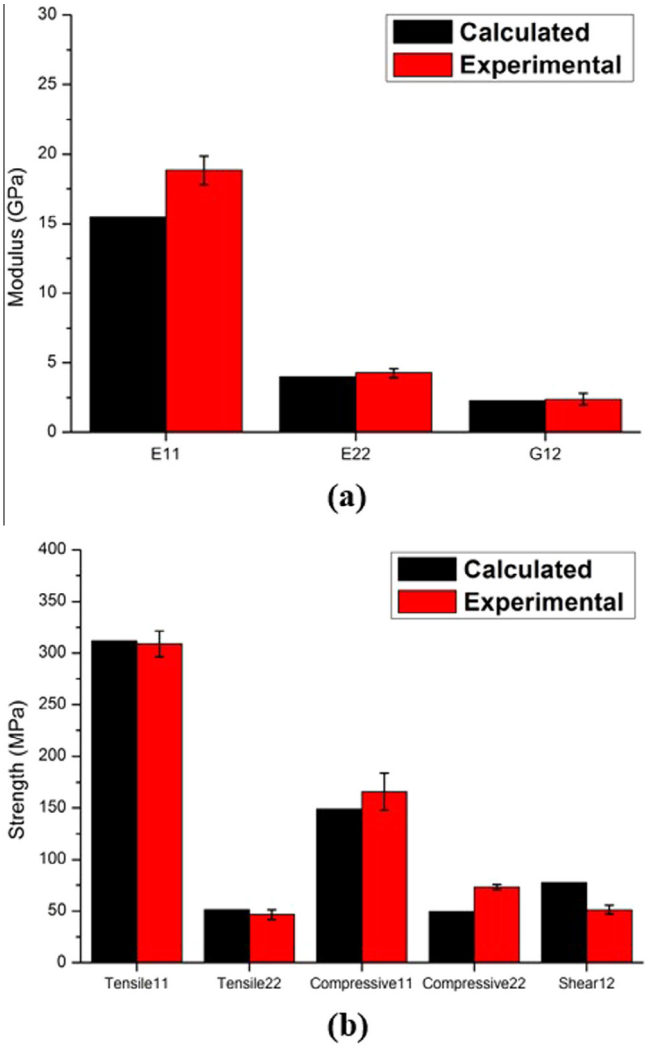

Fig. 10. Predicted mechanical properties of conventional GMT: (a) moduli; (b) strengths.

$$
\begin{array}{ll}
\textit{Find} & b,\ u_i,\ r_i,\ l_i \quad i = 1,\ 2,\ 3 \\
\textit{to minimize} & m_b \\
\textit{subject to} & [b, u_i, r_i, l_i] \in [3, 4, \ldots, 14] \quad i = 1,\ 2,\ 3 \\
 & \text{Intrusion} \leq 136\ \text{mm} \\
 & \text{Deflection} \leq 93.6\ \text{mm} \\
\textit{with} & \text{Material case} = 1,\ 2,\ 3,\ 4
\end{array}
\tag{18}
$$

4.3. Optimization method

In this work, the micro-genetic algorithm (μGA) was used to solve the discrete optimization problem with high computational efficiency. The μGA has been successfully employed to solve the discrete optimal design problems with accelerated convergence compared to the traditional genetic algorithm (GA) which has the serious limitation of severe computing time [24–28]. The μGA is the "small population" of GA that operates on the principles of natural selection or survival of the fittest to evolve the best potential solution over a number of generations to find the most-fit or optimal solution. During evaluation, the algorithm keeps the best individuality from the previous converged generations (elitism). Then, a new random population is chosen and the evolution process restarts. With a these procedures, the generation evolves and converges to a local optimal solution [26]. The μGA is better at distinguishing the global optimal solution from the local solution because it works with a population of strings while many optimization algorithms move from one point to another in the design variable space.

The procedure for the determination of optimal thickness of each part is as follows. First, the values of the design constraints (deflection and intrusion) and objective function (total weight of bumper beam) were obtained from LS-DYNA corresponding to the initial population of design variables. Then those values are evaluated and the remaining strings are determined using a tournament selection strategy. In this strategy, strings are paired randomly, and adjacent pairs compete to become the remaining strings in the following generation. In the following step, the next set of strings is obtained by the crossover operation. Using the new strings, the convergence of the population loop is verified. If the population loop has not converged, the selection and crossover operations are repeated until the population loop converges.

Finally, highest fitness values in the final generation is outputted as the solution of the optimization problem [26–28].

4.4. Final design of hybrid bumper beam

After the design optimization of hybrid bumper beam for each material case, the final design was chosen with considering of the total mass, impact performances and also the reinforced content of carbon fibers. Then, the hybrid bumper beam was manufactured based on the selected final design result. Fig. 9 shows the hot-press molding process for manufacturing of hybrid GCMT composite bumper beam supported by Hyundai Motors. Then, the impact test of manufactured bumper beam was performed based on IIHS standard and compared with the simulation results.

5. Results and discussion

Fig. 10 shows the mechanical properties of conventional GMT obtained by experiments and calculations explained in Section 2.

Table 3
Optimized designs of the GCMT bumper beam in each material case.

Designs	Parts	Top flange (u)	Lib (r)	Bottom flange (l)	Reinforcement (b)
Conventional	1	11.5	12	10.5	13
	2	11.5	11.5	10.5	
	3	10.5	10.5	10.5	
Case 1	1	9	7	6	11
	2	10	6	6	
	3	9	7	7	
Case 2	1	7	8	6	10
	2	7	5	7	
	3	6	7	6	
Case 3	1	8	6	8	10
	2	7	9	7	
	3	7	9	5	
Case 4	1	8	8	9	10
	2	6	9	4	
	3	5	9	7	

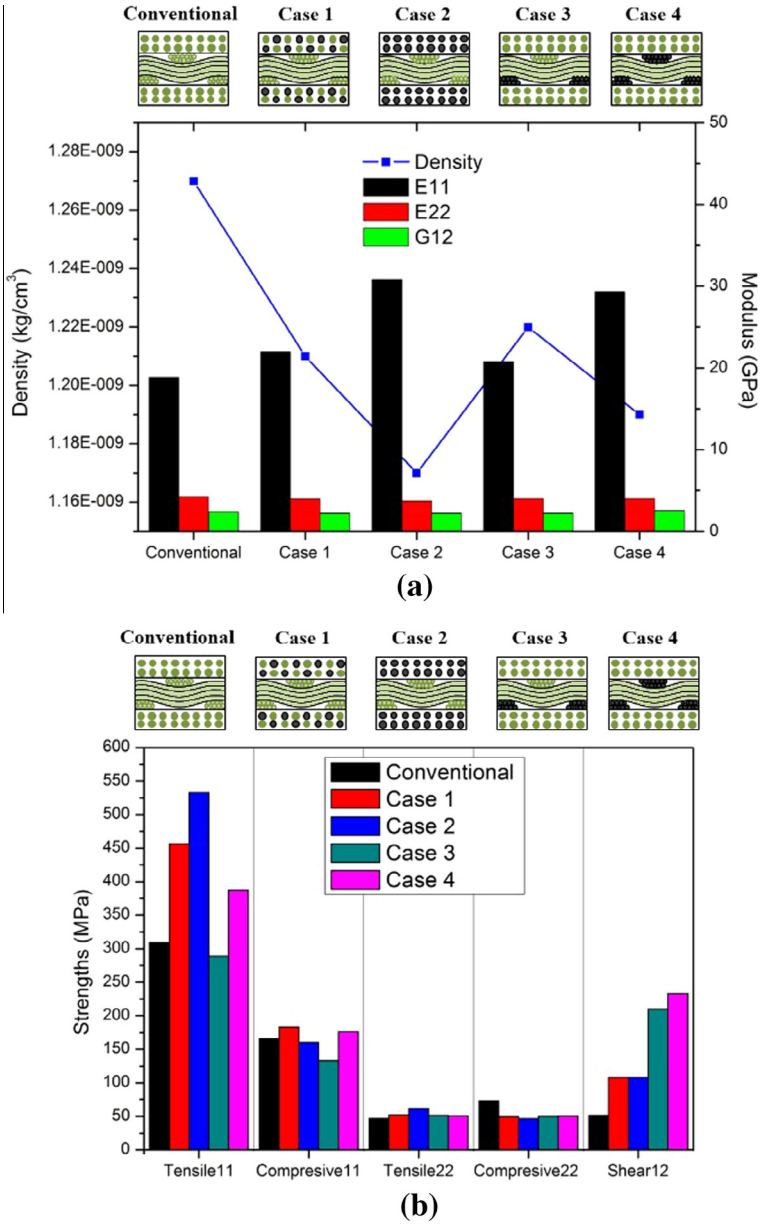

Fig. 11. Physical and mechanical properties of designed GCMT: (a) density and moduli; (b) strengths.

It was found that all of the calculated mechanical properties showed good agreements with the experimental results. The errors between the experiment and prediction might come from the voids or small defects generated during manufacturing process. Based on these results, it could be concluded that the mechanical properties of layered composite structures can be predicted well using CLPT method.

The mechanical properties of newly designed four types of GCMT (cases 1–4 of described Section 2.1) were also calculated and depicted as shown in Fig. 11. The density of all hybrid composites was reduced by substituting of glass fibers with carbon fibers. The lowest density was obtained from the case 2 because the most amount of glass fibers was replaced by carbon fibers (total 28 vf%). In the case of moduli, the longitudinal elastic modulus was increased for all of design cases due to the higher elastic modulus of carbon fiber compared to the glass fiber. Especially, almost 40% increased longitudinal elastic modulus were obtained in the case 2 and case 4 because the high volume fraction of carbon fiber (28 and 23 vf%, respectively) was reinforced. However, the transverse modulus and shear modulus showed similar value compared to those of conventional GMT. It is come from the fact that the transverse modulus and shear modulus are almost dependent on the mechanical properties of the matrix, not those of fiber [8].

In the case of strengths, the different improving trend could be found as the replacement position of carbon fiber as shown in Fig. 11b. The noticeable improvements of longitudinal tensile strength could be achieved only when the carbon fiber was reinforced in the UD layer (cases 1 and 2). It is come from the fact that the conventional UD layer is fractured earlier than the woven layer due to its lower tensile strength. On the other hand, in the cases of

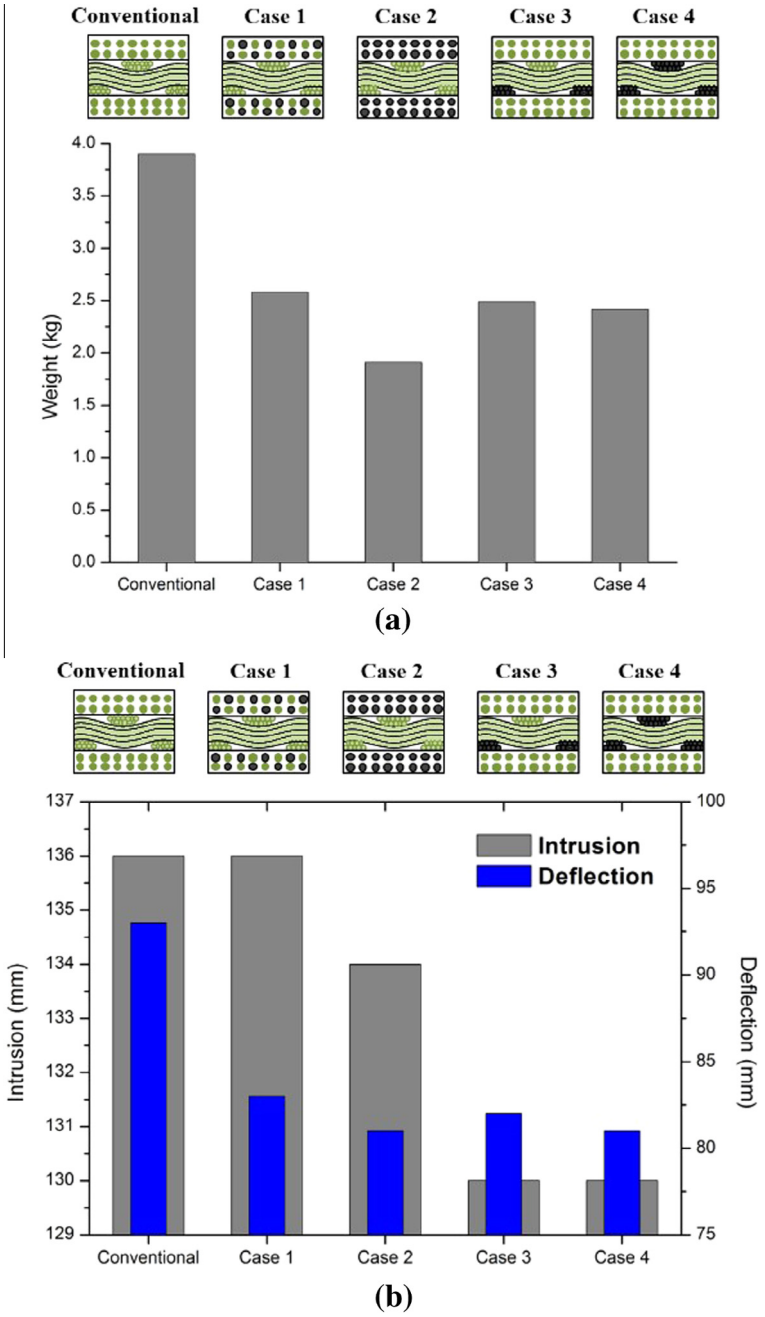

Fig. 12. Specification of optimally designed bumper beam with respect to material case: (a) weight; (b) impact performance.

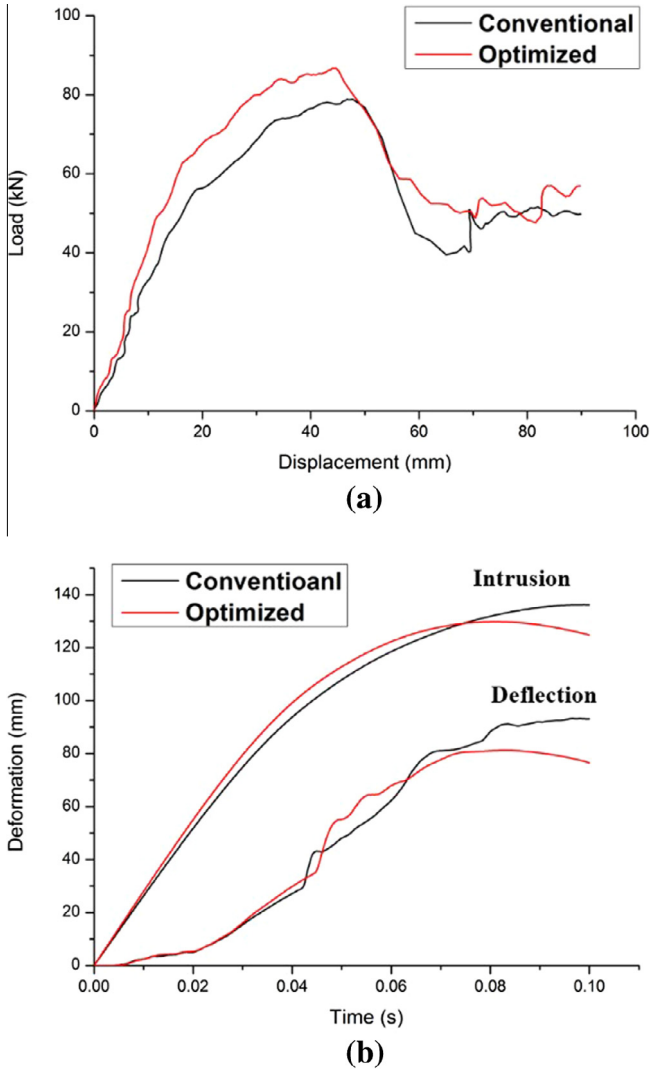

Fig. 13. Impact performances of the optimally designed hybrid GCMT composite bumper beam: (a) load–displacement curve; (b) deflection and intrusion with respect impact time.

3 and 4, it is noteworthy that the almost 4 times higher shear strength was achieved compare with that of the conventional GMT. It might be because the shear strength of woven layer was much improved by carbon fiber. In other words, the entire shear strength could be enhanced due to the increased shear strength of woven layer because the shear strength of entire GCMT is determined by lowest shear failure strength. However, in the case 4, the improving of shear strength was almost saturated although the 2 times higher amount of carbon fiber was reinforced. It is because that the shear strength of woven layer was increased more than that of UD layer thus the UD layer is fractured earlier than the woven layer due to its lower shear strength. In the case of compressive strengths and transverse tensile strength, there were only small changes because these properties are much dependent on the mechanical properties of matrix, not the properties of fiber [12]. Based on these results, it could be concluded that the tensile strength and shear strength of GCMT can be improved by the reinforcement of carbon fiber into the UD layer or woven layer, respectively. Using these properties, the optimal design of hybrid bumper beam could be performed for each material case with impact simulation as described in Section 4.

Table 3 shows the optimized thicknesses of bumper beam parts (Fig. 7d) in each material case. Also, the weight and impact performances of optimally designed bumper beam were obtained in each material case as shown in Fig. 12. It was found that all of the performances including weight, the intrusion and deflection were successfully improved by optimization using GCMT materials. Note that the cases 1 and 2 showed much higher intrusion than those in the cases of 3 and 4. It might be because the impact performance might be much dependent on the shear strength of GCMT rather than its tensile strength. Therefore, the results in case 3 and case 4 showed the best impact performances (the lowest deflection and intrusion) with about 1.4 kg of weight reduction due to its improved shear strength. Also, it is noteworthy that the only half amount of carbon fiber was replaced in the woven layer in the case 3 compared to the case 4. Therefore, considering the cost of carbon fiber, the optimal design using the material case 3 could be chosen as the final design for the hybrid bumper beam. Fig. 13 shows the impact simulation results of the final design of GCMT bumper beam. It could be confirmed that the maximum failure load was improved and the intrusion and deflection were reduced compared to the conventional bumper beam. Fig. 14 shows the manufactured hybrid bumper beam based on the final design and its impact test. After the impact test, the fracture positions were observed and compared to the results of impact

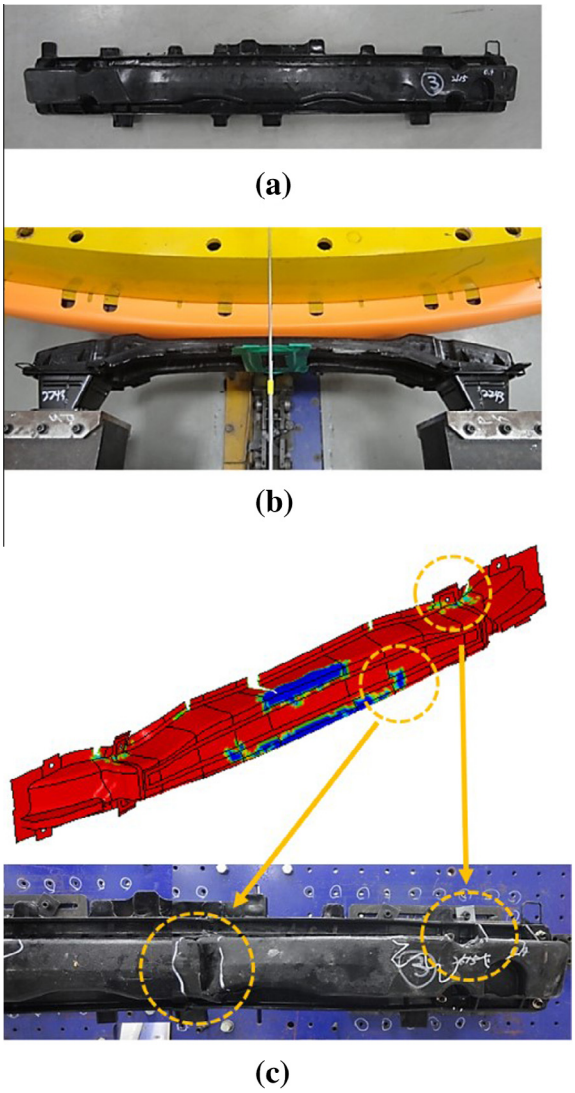

Fig. 14. Manufactured hybrid bumper beam and impact test: (a) finally designed hybrid bumper beam; (b) bumper impact test; (c) fracture of bumper beam after impact simulation and test.

Table 4
Final design results obtained from impact simulation and real test.

	Weight (kg)	Intrusion (mm)	Deflection (mm)
Simulated	2.49	130	82
Tested	2.61	123	89
Conventional	3.9	136	93

simulation (Fig. 14c). It could be found that the fractured area of manufactured GCMT bumper beam agreed well with the impact simulation result. The impact performance from the impact simulation and real impact test were described in Table 4. Although the weight of manufactured bumper beam had slightly heavier than the calculation, about 33% (1.3 kg) of the weight could be reduced and both of the intrusion and deflection were improved to be 123 mm and 89 mm compared to those of the conventional bumper beam (136 mm and 93 mm, respectively).

5. Conclusions

In this study, the various designs of glass/carbon mat thermoplastic (GCMT) were devised and its mechanical properties were calculated by classical laminates plate theory. Then, the GCMT bumper beam was optimally designed for each material case by using the μGA algorithm with the impact simulation. Based on the optimal design results, the final design of GCMT bumper beam was selected with considering of the weight, impact performances and used amount of carbon fiber. Then, the real bumper beam was manufactured by using the final design and its impact performances were measured. It was found that the optimally designed GCMT bumper beam had 33% less weight compared to the conventional GMT bumper beam while having the improved impact performances.

Acknowledgments

This work was supported by the Technology Innovation Program (or Industrial Strategic Technology Development Program, 10048913, Development of the cheap nano-ink which is sintered in the air for smart devices) funded by the Ministry of Trade, Industry & Energy (MI, Korea). This work was also supported by the National Research Foundation of Korea (NRF) funded by the Ministry of Education (Nos. 2012R1A6A1029029 and 2013M2A2A9043280).

References

[1] McAuley JW. Global sustainability and key needs in future automotive design. Environ Sci Technol 2003;37:5414–6.
[2] Badie MA, Mahdi E, Hamouda AMS. An investigation into hybrid carbon/glass fiber reinforced epoxy composite automotive drive shaft. Mater Des 2011;32:1485–500.
[3] Boria S, Belingardi G. Numerical investigation of energy absorbers in composite materials for automotive applications. Int J Crashworthiness 2012;17:345–56.
[4] Al-Qureshi HA. Automobile leaf springs from composite materials. J Mater Process Technol 2001;118:58–61.
[5] Botkin ME. Modelling and optimal design of a carbon fibre reinforced composite automotive roof. Eng Comput 2000;16:16–23.
[6] Li YX, Lin ZQ, Jiang AQ, Chen GL. Experimental study of glass-fiber mat thermoplastic material impact properties and lightweight automobile body analysis. Mater Des 2004;25:579–85.
[7] Hosseinzadeh R, Shokrieh MM, Lessard L. Damage behavior of fiber reinforced composite plates subjected to drop weight impacts. Compos Sci Technol 2006;66:61–8.
[8] Lee DG, Suh NP. Axiomatic design and fabrication of composite structures: applications in robots, machine tools and automobiles. New York, Oxford: Oxford University Press; 2006.
[9] Lee C, Hwang W. Modified rule of mixtures for prediction of tensile strength of unidirectional fiber-reinforced composites. J Mater Sci Lett 1998;17:1601–3.
[10] Naik NK, Kumar RS. Compressive strength of unidirectional composites: evaluation and comparison of prediction models. Compos Struct 1999;46:299–308.
[11] Davila CG, Camanho PP, Rose CA. Failure criteria for FRP laminates. J Compos Mater 2005;39:323–45.
[12] de Kok JMM, Peijs T. Deformation, yield and fracture of unidirectional composites in transverse loading: 2. Influence of fibre-matrix adhesion. Compos Part A – Appl Sci Manuf 1999;30:917–32.
[13] Shina PK. Composite materials and structures. Kharagpur: Department of Aerospace Engineering, Indian Institute of Technology; 1995.
[14] Khandan R, Noroozi S, Sewell P, Vinney J. The development of laminated composite plate theories: a review. J Mater Sci 2012;47:5901–10.
[15] Daniel I. Failure of composite materials. Strain 2007;43:4–12.
[16] Naik GN, Gopalakrishnan S, Ganguli R. Design optimization of composites using genetic algorithms and failure mechanism based failure criterion. Compos Struct 2008;83:354–67.
[17] Low-speed crash test protocol. Insurance Institute for Highway Safety; 2006.
[18] Herranen H, Pabut O, Eerme M, Majak J, Pohlak M, Kers J, et al. Design and testing of sandwich structures with different core materials. Mater Sci 2012;18:45–50.
[19] Majak J, Pohlak M, Eerme M, Velsker T. Design of car frontal protection system using neural network and genetic algorithm. Mechanics 2012;18:453–60.
[20] Pohlak M, Küttner R, Majak J. Modelling and optimal design of sheet metal RP&M processes. Rapid Prototyping J 2005;11:304–11.
[21] Park DK. A development of simple analysis model on bumper barrier impact and new IIHS bumper impact using the dynamically equivalent beam approach. J Mech Sci Technol 2011;25:3107–14.
[22] Deb A, Naravane A, Chirwa EC. An offset rigid barrier-based test: equivalence to the insurance institute for highway safety frontal offset impact safety test. Int J Crashworthiness 2006;11:281–90.
[23] Groenwold AA, Haftka RT. Optimization with non-homogeneous failure criteria like Tsai-Wu for composite laminates. Struct Multidiscip Optim 2006;32:183–90.
[24] Wang Q, Fang HB, Zou XK. Application of Micro-GA for optimal cost base isolation design of bridges subject to transient earthquake loads. Struct Multidiscip Optim 2010;41:765–77.
[25] Kim DH, Choi DH, Kim HS. Design optimization of a carbon fiber reinforced composite automotive lower arm. Compos Part B – Eng 2014;58:400–7.
[26] Krishnakumar K. Micro-genetic algorithms for stationary and non-stationary function optimization. Proc SPIE 1196, Intell Control Adapt Syst 1990:289–96.
[27] Chakravarty S, Mittra R, Williams NR. On the application of the microgenetic algorithm to the design of broad-band microwave absorbers comprising frequency-selective surfaces embedded in multilayered dielectric media. IEEE Trans Microw Theory Tech 2001;49:1050–9.
[28] Yan G, Zhou L. Impact load identification of composite structure using genetic algorithms. J Sound Vib 2009;319:869–84.